International Communications in Heat and Mass Transfer 179 (2026) 112127

Contents lists available at ScienceDirect

International Communications in Heat and Mass Transfer

journal homepage: www.elsevier.com/locate/ichmt

Asymmetric melting–solidification in horizontal latent thermal energy storage: Impact of fins location and of natural convection

Claudia Naldi [a,*], Giulia Martino [a], Cesare Biserni [a], Sylvie Lorente [b]

[a] Department of Industrial Engineering, University of Bologna, Viale del Risorgimento 2, 40136 Bologna, Italy
[b] Mechanical Engineering Department, Villanova University, 800 Lancaster Ave., Villanova, PA 19085, USA

ARTICLE INFO

Keywords:
Latent thermal energy storage
Phase change material
Metallic fins
Enhanced heat transfer

ABSTRACT

This paper presents a theoretical–numerical investigation of melting–solidification cycles in a horizontal latent thermal energy storage (LTES) system enhanced by metallic fins and natural convection. The storage is made of a double rectangular cavity filled with octadecane, separated by a central heat transfer fluid channel. Four fin arrangements are analyzed: no fins, fins in the upper cavity, fins in the lower cavity, fins in both cavities. The finite element numerical model is based on the apparent heat capacity method for phase change, accounting for conduction–convection interactions.

The results highlight that melting is dominated by natural convection in the upper cavity and conduction in the lower one, while solidification remains largely conduction-controlled, emphasizing the strong asymmetry between melting and solidification driven by buoyancy effects. Adding metallic fins significantly enhances the phase change processes; yet their effectiveness strongly depends on their location. Fins in the upper cavity accelerate local melting but do not reduce the total cycle time, because it is governed by the lower cavity. Conversely, fins in the lower cavity substantially improve overall performance by accelerating the limiting phase change process. The configuration with fins in both cavities yields the shortest cycle time.

A comparison between full-cycle and partial-cycle strategies shows that early switching between melting and solidification significantly reduces the cycle duration but comes with a reduction in total heat exchanged. The presented outcomes provide physical insight into the impact of fins placement and operating strategies, offering guidelines to design more efficient and cost-effective LTES systems.

1. Introduction

The continuously growing energy demand has made the need for efficient energy storages one of the most pressing challenges. Many researchers actively developed methods to reduce energy consumption and enhance the energy efficiency of HVAC (Heating, Ventilation and Air Conditioning) systems. In particular, Latent Thermal Energy Storage (LTES) systems have attracted significant attention due to their ability to store and release large quantities of thermal energy thanks to the latent heat of fusion of appropriate Phase Change Materials (PCMs) [1]. Despite this, the low thermal conductivity of PCMs slows down both the melting and solidification processes in this type of system. Consequently, several strategies are proposed in the literature to enhance the thermal conductivity of PCMs, ensuring the fast distribution of heat from the heat transfer fluid within the phase change material. In particular, solutions offer the incorporation of metallic fins [2,3] the use of metal foams [4,5], the addition of nanoparticles [6], design modifications [7–9], and the introduction of rotational effects [10].

Due to its simplicity, cost-effectiveness, and efficiency, the strategy of adding fins has been widely employed. For instance, Shen et al. [11] numerically analyzed the effect of fin angle, fin length, and fin number on heat radiation during the charging process of a shell and tube LTES unit. Their results showed that the increase in the fin number or fin length reduces the role of thermal radiation. In addition, the melting rate is enhanced by reducing the fin angle, extending the fin length, or increasing the fin number. Also Kim et al. [12] analyzed a shell and tube LTES featuring different designs and found that the finned multitube configuration improves temperature uniformity and reduces the melting and solidification times by about 90% compared to single tube design.

Abbreviations: HTF, Heat Transfer Fluid; HVAC, Heating, Ventilation and Air Conditioning; LTES, Latent Thermal Energy Storage; PCM, Phase Change Material; RMSD, Root Mean Square Deviation.

* Corresponding author.
E-mail address: claudia.naldi2@unibo.it (C. Naldi).

https://doi.org/10.1016/j.icheatmasstransfer.2026.112127

Available online 25 July 2026

Nomenclature

c_p	Specific heat capacity at constant pressure, J/(kg K)
$\vec{g}$	Gravitational acceleration vector, m/s^2
H	Storage tank height, m
h	Height of the heat transfer fluid channel, m
h_f	Fins height, m
k	Thermal conductivity, W/(m K)
L	Storage tank length, m
L_f	Latent heat of fusion, J/kg
p	Pressure, Pa
Q	Heat, J
Re	Reynolds number
T	Temperature, K
t	Time, s
t_f	Fins thickness, m
V	Volume, m^3
$\vec{v}$	Velocity vector, m/s
W	Storage tank width, m

Greek letters

β	Thermal expansion coefficient, 1/K
δ	Melt layer thickness
θ	Liquid fraction
μ	Dynamic viscosity, Pa s
ρ	Density, kg/m^3

Superscripts

–	Average
*	Non-dimensional

Subscripts

C	Cold
c	Copper
ex	Exchanged
f	Fins
fr	Fraction
H	Hot
h	Higher
L	Latent
l	Lower
m	Modified
pc	Phase change
S	Sensible
TOT	Total
$trans$	Transition

Srivastava and Rekha Sahoo [13] performed a computational study on a PCM melting in a triple-tube thermal energy storage, where a segmented multi-PCM system fills the intermediate annulus. The authors showed that longitudinal fins enhance convective melting and decrease by about 20% the total melting time compared to radial fins. Ren et al. [14] proposed an irregular snowflake-shaped fin structure to improve the melting performance of a horizontal LTES unit. The results revealed that this innovative fin structure reduces the melting time by 45.92%. Arshad [15] conducted a parametric study on a PCM-based tree-shaped finned heat sink and evaluated the phase change time and heat transfer mechanisms involved. The obtained results show that both the height of the tree-shaped fins and the number of branches or twigs strongly influence the heat transfer rate, for a constant volume fraction. Amer et al. [16] studied the effectiveness of hook-shaped fins in comparison to traditional straight fins, showing that the proposed design considerably improves the thermal response of the system, reducing charging times by up to 58.6%. Xiao et al. [17] investigated the design of a rectangular finned LTES unit with multiple cavities, demonstrating how the multi-cavity fin improves heat transfer thanks to the networked conductive paths, despite natural convection suppression.

Numerous studies have analyzed the melting and solidification processes of PCMs in several encapsulation geometries, including spheres [18] and rectangular enclosures [19]. In particular, Ge et al. [20] analyzed the performance improvement achievable by adding fins in spherical capsules containing a PCM. Their experimental results confirmed that increasing the number of fins enhances the thermal storage and release capacities by up to 151.1% compared to the no-fin case. The authors also showed that the efficiency of the fins is up to 25% higher in the thermal discharge process than in the charging process.

Three-dimensional numerical simulations were conducted by Liu et al. [21] to investigate the influence of the addition of longitudinal fins near the bottom of a rectangular enclosure filled with the PCM RT42 and heated from one side. The authors stated that adding longitudinal fins at the bottom of the cavity improves the temperature uniformity and facilitates natural convection. Moreover, greater fin thickness reduces the melting rate and further enhances buoyancy convection, leading to a more significant performance improvement compared to the baseline case.

The thermal storage shape and orientation also play an important role in the optimization of the system performance. In an experimental study conducted by Lu et al. [22], the effect of shell shape on the charging and discharging performance of a vertical LTES unit was investigated. The authors designed and fabricated a cylindrical and two conical vertical LTES units. The results demonstrated that the conical units reduce the entire melting/solidification time by up to 29.94%, and the time-averaged heat transfer rate increases by up to 41.24% compared to the cylindrical unit. Medjahed et al. [23] conducted an experimental study to evaluate the thermal performance of a small-scale LTES using beeswax as the PCM within a horizontal shell and tube heat exchanger. Their findings showed that the discharging duration is considerably longer than the charging time, due to the gradual formation of a solid PCM layer around the outer surface of the heat exchanger during the discharge procedure. Among the various LTES designs, the choice between vertical and horizontal configurations is influenced by several design constraints and technical issues [24–26].

The literature analysis evidences the benefits of fins inclusion on the thermal performance of LTES systems. However, a comprehensive study on the effects of fins positioning within horizontal latent thermal energy storages and on the corresponding heat transfer mechanisms involved in both the PCM melting and solidification processes is still missing to the authors' knowledge.

In this study, a horizontal LTES system consisting of a double rectangular cavity filled with PCM and heated/cooled from the center is analyzed. Numerical simulations are conducted to investigate the heat transfer phenomena during the PCM melting and solidification. The addition of metallic fins in the upper, lower, or both cavities is considered in order to evaluate the impact of metallic inclusions on the efficiency of the energy stored and released. Different melting and solidification cycles are considered to investigate the influence of the fins location on the time needed to complete the phase change process and on the thermal energy accumulated/delivered by the system. The presented findings can represent helpful guidance to support the design of new efficient and cost-effective latent thermal energy storage systems.

2. Case study

The horizontal latent thermal energy storage considered is composed of a double cavity, filled with a PCM, either with or without a certain number of metallic fins. The storage tank is parallelepipedal and the heat transfer fluid flows from one side to the opposite one through a thin horizontal plenum that separates completely the system into upper and lower cavities of rectangular cross sections. It is next assumed that the third dimension is long enough to consider a two-dimensional problem, as shown in Fig. 1. The studied configurations are: i) bare storage tank (Fig. 1a); ii) storage tank with fins in the upper cavity only (Fig. 1b); iii) storage tank with fins in the lower cavity only (Fig. 1c); iv) storage tank with fins in both cavities (Fig. 1d).

In each configuration, heat is being exchanged between the heat transfer fluid placed in the horizontal channel between the two cavities and the PCM, subjected to phase change. The following cycles are considered: i) total melting and total solidification, namely melting takes place until the entire volume of the storage tank is fully melted, followed by solidification of the entire storage tank volume; ii) single cavity-melting and single cavity-solidification, namely melting occurs until one of the two cavities completes the phase change, then solidification follows until one of the two cavities completes the phase change.

In order to compare the effect of the different fins configurations on the system efficiency, results of each studied case are presented in terms of heat transfer mechanisms (*i.e.*, conduction or convection), average liquid fraction evolution, time needed to complete the phase change, and total thermal energy exchanged.

3. Numerical strategy

3.1. Geometry, materials and governing equations

The storage unit is a parallelepiped of length L, width W and height H (see Fig. 1). As mentioned, the width W is such that $W \gg L$ and $W \gg H$, justifying the two-dimensional assumption taken in this work. At mid-height a thin channel of height h and width W allows the heat transfer fluid to flow along the distance L and exchange heat with the phase change material (PCM) that fills the storage tank. It is considered that the temperature of the heat transfer fluid remains at a constant and uniform value during the melting (T_H) and solidification (T_C) processes. A validation of this assumption is reported in Appendix A. All the walls of the storage unit are insulated. Several cases are considered. First, the tank is entirely filled with PCM. Then metallic fins of height h_f, thickness t_f and width W are added, either in the top section of the storage unit, or in the bottom part, or in both. The fins are connected to the channel where the heat transfer fluid flows. The other end is not in contact with the tank wall $\left(h_f < (H-h)/2\right)$, allowing PCM circulation when in liquid state, because the aim is not to transfer heat from the central channel to the tank walls, but to store and release thermal energy through PCM melting and solidification [27]. There are six fins per side, separated by the same distance in each case. The selected fin configuration provides sufficient heat transfer enhancement in the PCM without excessively reducing the PCM volume or significantly hindering the convective cells that occur during PCM melting [27]. The change in PCM volume is from 0.00780 m^3 (0 fins) to 0.00752 m^3 (12 fins) with the numerical values here considered. Accordingly, the volume fraction V_{fr}, namely the ratio between the fins' volume and the total volume of the cavities, ranges from 0 (0 fins) to 0.0359 (12 fins).

The problem is described by the mass, momentum and energy conservation equations given below:

$$\nabla \cdot \vec{v} = 0 \tag{1}$$

$$\rho \frac{\partial \vec{v}}{\partial t} + \rho(\vec{v} \cdot \nabla)\vec{v} = -\nabla p + \mu \nabla^2 \vec{v} + \rho \vec{g} - \theta \rho \beta \left(T - T_{pc,l}\right) \vec{g} \tag{2}$$

$$\frac{\partial T}{\partial t} + (\vec{v} \cdot \nabla) T = \frac{k}{\rho c_{p,m}} \nabla^2 T \tag{3}$$

where $\vec{v}$ is the velocity vector, ρ is the PCM density, t is the time, p is the pressure, μ is the PCM dynamic viscosity, $\vec{g}$ is the gravitational acceleration vector, θ is the PCM local liquid fraction, β is the PCM thermal expansion coefficient, T is the temperature, $T_{pc,l}$ is the lower limit of the PCM phase change temperature range, $c_{p,m}$ is the modified specific heat capacity, and k is the PCM thermal conductivity.

In order to model the PCM phase change, the apparent heat capacity formulation is adopted [27,28]. The values of density, thermal conductivity and specific heat capacity of the PCM considered in this work do not change between solid phase and liquid phase as explained in previous studies [27,29,30]. The apparent heat capacity formulation requires the modified specific heat capacity $c_{p,m}$ in the energy conservation equation:

$$c_{p,m} = c_p \text{ if } T < T_{pc,l} \text{ (solid phase) or } T > T_{pc,h} \text{(liquid phase)} \tag{4}$$

$$c_{p,m} = c_p + \frac{L_f}{T_{pc,h} - T_{pc,l}} \text{ if } T_{pc,l} < T < T_{pc,h} \text{ (mushy region)} \tag{5}$$

where c_p is the PCM specific heat capacity, $T_{pc,h}$ is the higher limit of the PCM phase change temperature range, and L_f is the PCM latent heat of fusion.

The PCM local liquid fraction θ is a dimensionless parameter that

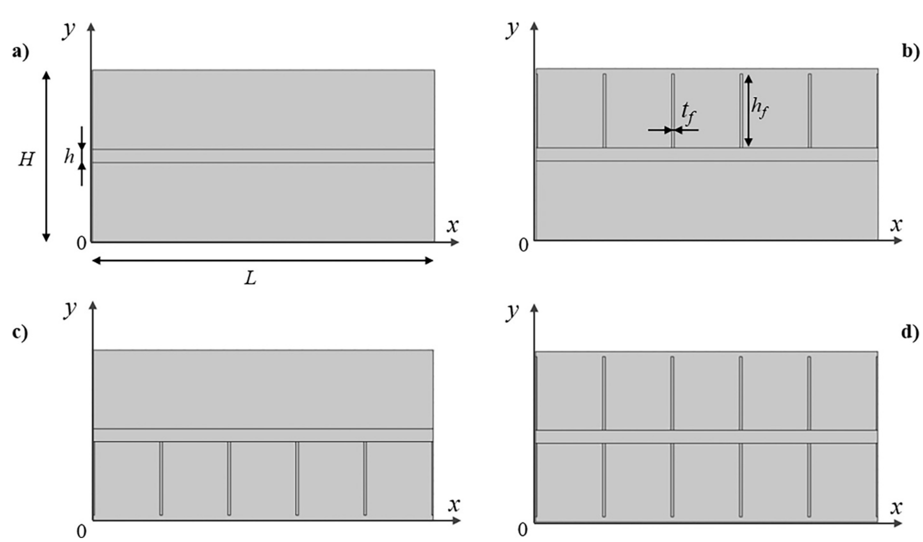

Fig. 1. Investigated geometries of the storage tank: a) no fins; b) fins in the upper cavity; c) fins in the lower cavity; d) fins in both cavities.

evaluates the PCM phase [31]:

$$\theta = 0 \text{ if } T < T_{pc,l} \text{ (solid phase)} \tag{6}$$

$$\theta = 1 \text{ if } T > T_{pc,h} \text{ (liquid phase)} \tag{7}$$

$$\theta = \frac{T - T_{pc,l}}{T_{pc,h} - T_{pc,l}} \text{ if } T_{pc,l} < T < T_{pc,h} \text{ (mushy region)} \tag{8}$$

If the storage tank includes metallic fins (cases of Fig. 1b–d), conduction is the mechanism for heat transfer along the fins, and the energy conservation equation is:

$$\frac{\partial T}{\partial t} = \frac{k_f}{\rho_f c_{p,f}} \nabla^2 T \tag{9}$$

where k_f, ρ_f and $c_{p,f}$ are the fins thermal conductivity, density and specific heat capacity, respectively.

The initial condition is given by:

$$T(x, y, 0) = T_{pc,l} \tag{10}$$

$$\vec{v}(x, y, 0) = 0 \tag{11}$$

The boundary conditions are:

$$\left.\frac{\partial T}{\partial x}\right|_{x=0} = \left.\frac{\partial T}{\partial x}\right|_{x=L} = \left.\frac{\partial T}{\partial y}\right|_{y=0} = \left.\frac{\partial T}{\partial y}\right|_{y=H} = 0 \tag{12}$$

$$T\left(x, \frac{H-h}{2}, t\right) = T\left(x, \frac{H+h}{2}, t\right) = T_H \text{ for melting process} \tag{13}$$

$$T\left(x, \frac{H-h}{2}, t\right) = T\left(x, \frac{H+h}{2}, t\right) = T_C \text{ for solidification process} \tag{14}$$

$$\vec{v}(0, y, t) = \vec{v}(L, y, t) = \vec{v}(x, 0, t) = \vec{v}(x, H, t) = 0 \tag{15}$$

Numerical simulations were performed with a finite element software [32] by considering the geometrical dimensions reported in Table 1. Octadecane is selected as PCM, fins are made of aluminum, and the heat transfer fluid channel is made of copper (material properties are shown in Table 2). The heat transfer fluid is at a constant temperature $T_H = 320$ K during the melting process and $T_C = 286$ K during the solidification process.

3.2. Mesh sensibility analysis

An unstructured triangular mesh, with finer elements near the walls, was chosen to discretize the computational domain. The independence of the results from the grid was tested by selecting three different mesh sizes, for the cases with no fins, fins in the lower cavity, and fins in both cavities, and by comparing the values of the liquid fraction $\overline{\theta}$, averaged over the domain, as a function of time. The $\overline{\theta}$ maximum absolute error and root mean square deviation are reported in Table 3. The analysis of the results indicates that the second mesh exhibits good performance for each considered domain, leading to selecting it.

Simulations were run with an absolute tolerance factor of 0.1 and a relative tolerance of 0.01. The computational time step was automatically refined, and the results were recorded every second. A simulation of 26,000 s required about 7 h on a PC with Intel Core i7-6700K, 4.0 GHz, 64 GB RAM.

Table 1
Geometric parameters of the storage tank.

Parameter	Dimensions [cm]
Storage tank length, L	13.0
Storage tank height, H	6.5
Heat transfer fluid channel height, h	0.5
Fins height, h_f	2.8
Fins thickness, t_f	0.1

Table 2
Materials thermophysical properties.

PCM: octadecane [29]	
Phase change temperature range, $T_{pc,l} - T_{pc,h}$ [K]	303–304
Thermal conductivity, k [W/(m K)]	0.2
Latent heat of fusion, L_f [kJ/kg]	125
Density, ρ [kg/m^3]	800
Specific heat capacity at constant pressure, c_p [kJ/(kg K)]	1.25
Dynamic viscosity, μ [Pa s]	0.008
Thermal expansion coefficient, β [1/K]	0.002
Fins: aluminum	
Thermal conductivity, k_f [W/(m K)]	237
Density, ρ_f [kg/m^3]	2700
Specific heat capacity at constant pressure, $c_{p,f}$ [kJ/(kg K)]	0.897
Heat transfer fluid channel: copper	
Thermal conductivity, k_c [W/(m K)]	390
Density, ρ_c [kg/m^3]	8920
Specific heat capacity at constant pressure, $c_{p,c}$ [kJ/(kg K)]	0.385

Table 3
Maximum absolute error and root mean square deviation for the average liquid fraction with different grids.

	Mesh	N. of elements	$\overline{\theta}$ maximum absolute error	$\overline{\theta}$ root mean square deviation
No fins	1	8182	0.06268	0.02723
	2	17,068	0.01635	0.00398
	3	17,562	–	–
Fins in the lower cavity	1	9924	0.05098	0.03488
	2	24,791	0.01498	0.00501
	3	25,061	–	–
Fins in both cavities	1	15,794	0.07482	0.02745
	2	32,562	0.00960	0.00384
	3	32,898	–	–

3.3. Validation of the model

The model validation was presented in our previous work [27] by comparing our results with those published by Guo et al. [33] and by Biwole et al. [34]. For a more comprehensive analysis, here we also compare our outcomes with those by Kiyak et al. [35], who studied the melting and solidification processes of a PCM filling an energy storage unit with different geometries and with different heater/cooler positions. For the sake of comparison, we selected the case of a square energy storage unit with melting/solidification from the bottom and adiabatic lateral and top walls.

Fig. 2 shows the average melting fraction $\overline{\theta}$ as a function of time, obtained with our model and by [35]. The initial increasing trend of $\overline{\theta}$ from $t = 0$ s to $t = 300$ s refers to the melting process, whilst the subsequent decreasing trend from $t = 300$ s to $t = 600$ s refers to the solidification process.

The agreement between our results and those by [35] is good: the maximum absolute error in the values of $\overline{\theta}$ is 0.05672 and the root mean square deviation is 0.01542, allowing to consider our model as validated.

4. Results and analysis

4.1. Total melting and total solidification

The complete cycle made of the full melting of the container followed by its full solidification is presented in Fig. 3 in terms of average melting fraction.

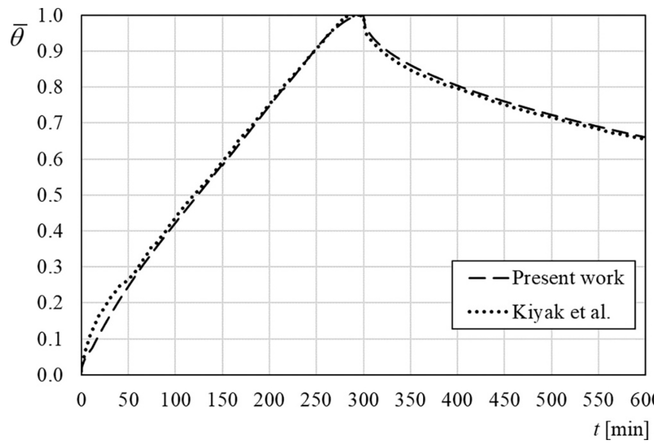

Fig. 2. Average melting fraction as a function of time, results by the present work and by [35].

While the shortest cycle time is obtained as expected when fins are added in the upper and lower cavities, Fig. 3 shows that adding fins in the upper cavity only does not allow to shorten the melting-solidification cycle duration. The changes in slope for a given configuration are dictated by the presence of fins and their impact changes depending on their location in the storage system.

A closer look into each configuration is presented in Figs. 4–8.

In Fig. 4, the melting of the storage tank without any fin is characterized by two different slopes. From $t = 0$ s to $t = 2900$ s, the PCM melts in both cavities but the melting mode differs between them as the PCM in the upper cavity melts quickly by convection, while in the lower cavity PCM melts by conduction heat transfer. Indeed, conducting a scale analysis of the melting front propagation [27], we showed previously that after heat is initially transferred by conduction between a bottom heated cavity and PCM, convection becomes the dominant heat transfer mode when time exceeds the transition value t_{trans}, defined as

$$t_{trans} \sim 100\left(\frac{k\Delta T}{\rho L_f}\right)^{-1}\left(\frac{g\beta\Delta T}{\nu\alpha}\right)^{-\ 2/3} \tag{16}$$

where t_{trans} is the transition time between conduction and convection heat transfers, and ΔT is the temperature difference between the heat transfer fluid and the lower limit of the melting temperature range.

The corresponding melt layer thickness is

$$\delta_{trans} \sim 10\left(\frac{g\beta\Delta T}{\nu\alpha}\right)^{-\ 1/3} \tag{17}$$

Fig. 5 shows the evolution of the computed melting front in time and the predicted transition location. Before transition, the melting front progresses upward as $t^{1/2}$, characteristic of a diffusion process (conduction heat transfer). As time increases, conduction is not sufficient to convey the heat from the bottom to the rest of the cavity and convection takes over, leading to the linear variation of the melting front with time. Note the good prediction of the transition obtained with scale analysis.

In Fig. 4, the change in slope during melting occurs when the top cavity is entirely filled with liquid. At this time, the melting fraction is 1 in the top half of the bottom cavity, the lower half being still solid. The PCM continues to melt, but at a much lower pace because the only heat transfer mode is conduction as the heat transfer fluid channel is located at the top of the cavity.

Once all the PCM is in liquid state, the temperature of the heat transfer fluid in the central channel is suddenly brought to $T_C =$ constant and the entire cavity starts solidifying. Fig. 6 shows the temperature distribution at the end of melting (right before setting the heat transfer fluid at T_C), at an intermediary time and at the end of the complete solidification process. At the end of melting, most of the top cavity is at the heat transfer fluid temperature, way beyond the PCM melting temperature, indicative of sensible heating. The PCM in the bottom cavity is at its melting temperature as heat exchange was through latent heat. This is why the initial conditions of solidification are different between the two cavities. Nevertheless, at approximately half of the total solidification time, a quasi-symmetrical behavior is observed. It is considered that solidification is complete as soon as the melting fraction becomes null in both cavities. This choice prevents the PCM temperature to get back to the initial condition (lower temperature value of the melting range) throughout the entire cavity. The time to solidify the PCM in the upper cavity is 14,019 s and it takes 13,501 s to solidify the PCM in the bottom one, which makes a difference between the two of about 4%.

We show in Fig. 7 the results obtained with fins in the upper cavity. The first melting sequence ends faster than in the previous configuration, at $t = 890$ s, thanks to the presence of the fins. A few seconds before the PCM in this upper cavity melts entirely, we note what we called in previous work [27] the presence of solid drops: each portion of PCM

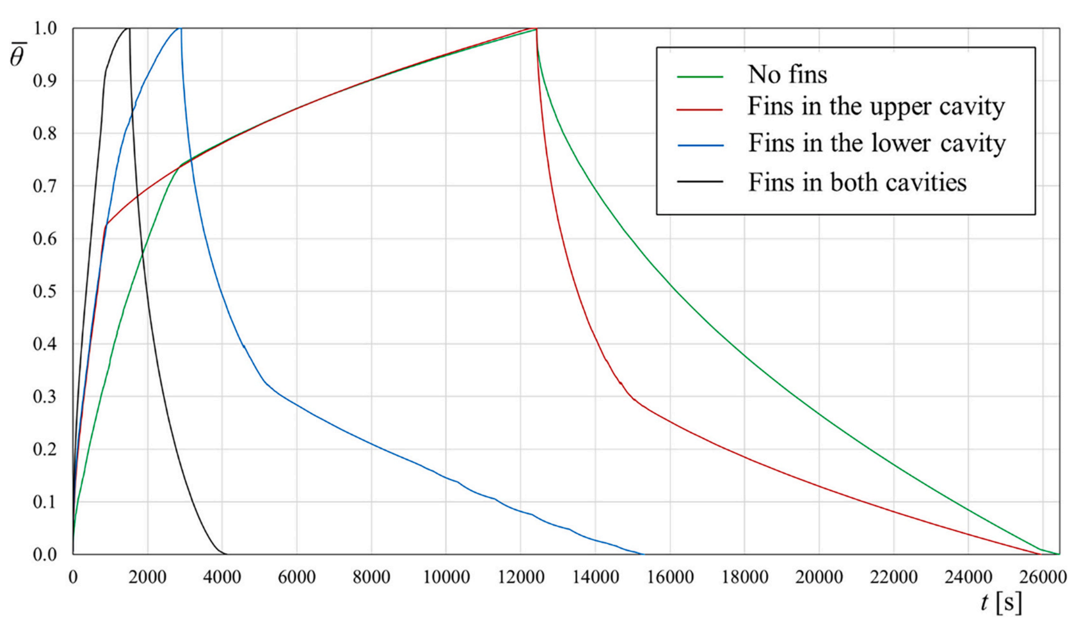

Fig. 3. Average melting fraction as a function of time, for different fins positions.

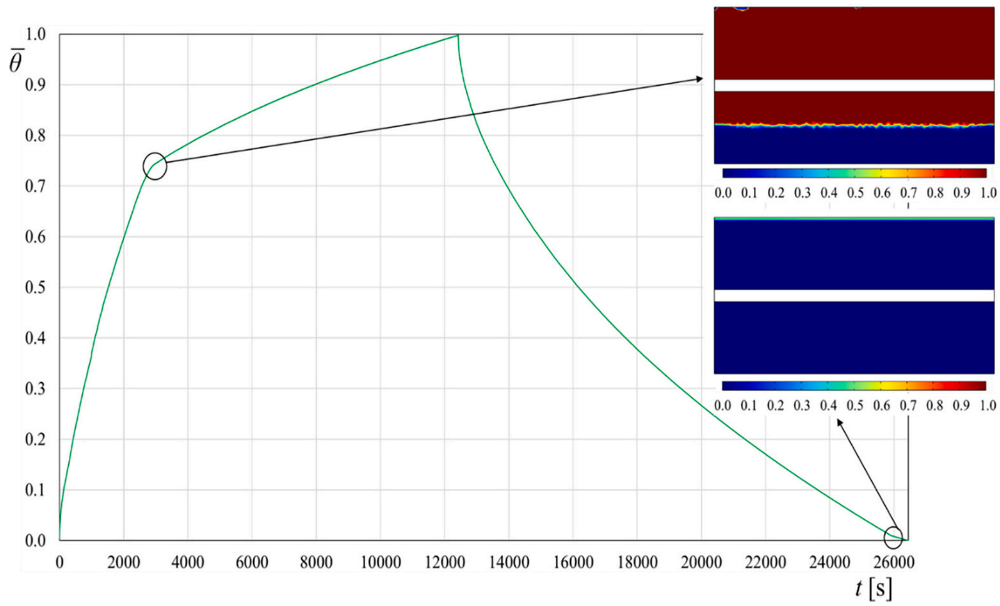

Fig. 4. No fins configuration; average melting fraction as a function of time and melting fraction distribution at significant instants.

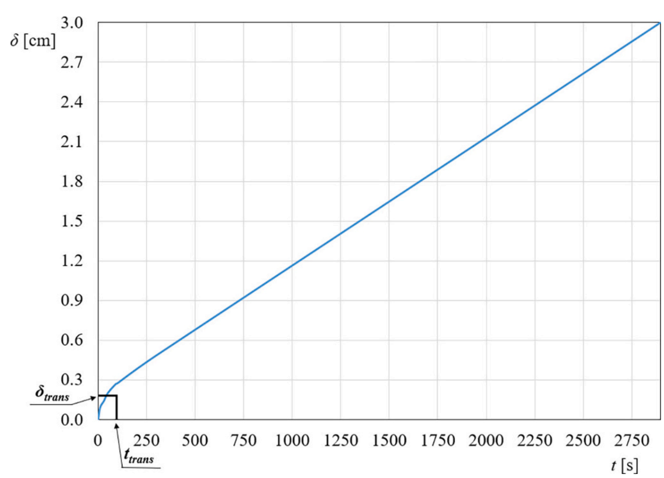

Fig. 5. No fins configuration; time evolution of the melting front for the upper cavity and transition location between conduction and convection predicted by the scale analysis.

delineated by two vertical fins is heated at the bottom and by the two fins. The horizontal liquid boundary layer generated in the vicinity of the horizontal channel propagates towards the top of the cavity. In the meantime, vertical boundary layers develop along the fins and their thickness increases with height. The combination of those three boundary layers, a horizontal one and two vertical ones, leads to entrapping a portion of solid PCM, the shape of which is similar to a drop as shown in Fig. 7 (bottom left).

In time, thanks to shear stresses generated by the PCM downward liquid movement at the interface liquid/solid, the solid drop falls and finishes melting while in the vicinity of the hot horizontal channel. Note that the driving forces generating the fall of the solid drops are the shear forces and not gravity because in this work the liquid PCM density is equal to the solid phase density. During the solidification phase, the fins are considered to be immediately at the same temperature as the central horizontal plenum, T_C, due to their high thermal conductivity [27].

Even though at the end of melting the PCM in the top cavity is at the heat transfer fluid temperature, as in the no fins configuration, the presence of the fins allows to solidify faster as they are brought at the cold temperature at the same time as the heat transfer fluid. This is indicated by the sharp decreasing slope of the melt fraction during the first part of solidification. When solidification is complete in the top cavity, the PCM is solidified in the low one until mid-height as shown in Fig. 7 (bottom right image). While the presence of fins enhances melting and helps solidification in the top cavity, the total melting and solidification times are identical to the no fins configuration because the lower cavity dictates the time for melting and solidifying.

In the case of fins in the downside of the storage tank (Fig. 8, blue curve), the total melting time is the one corresponding to the melting of the top cavity. Indeed, the bottom cavity melts quicker thanks to the presence of fins. Vertical boundary layers develop along the fins and accelerate the transversal propagation of heat, allowing the PCM to melt faster than without fins. The solid phase is trapped between the insulated cavity bottom, the PCM melted along the fins and the top, creating a dome shape between each compartment. These solid domes shrink as the horizontal melting front progresses downward.

The solidification time in the upper cavity is faster than in the no fins configuration (12,409 s instead of 14,059 s). This is due to a different

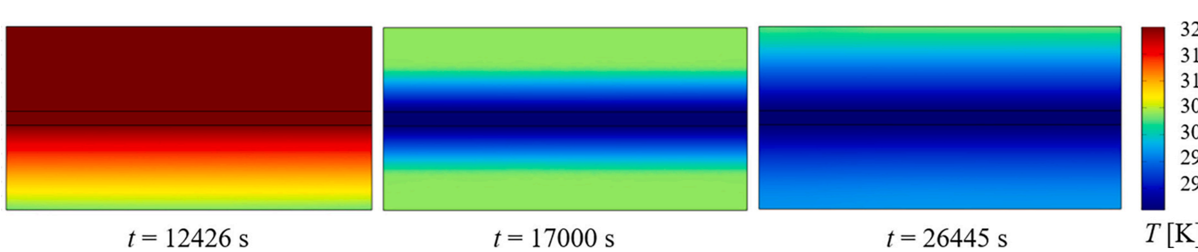

Fig. 6. No fins configuration; time sequence of the solidification process.

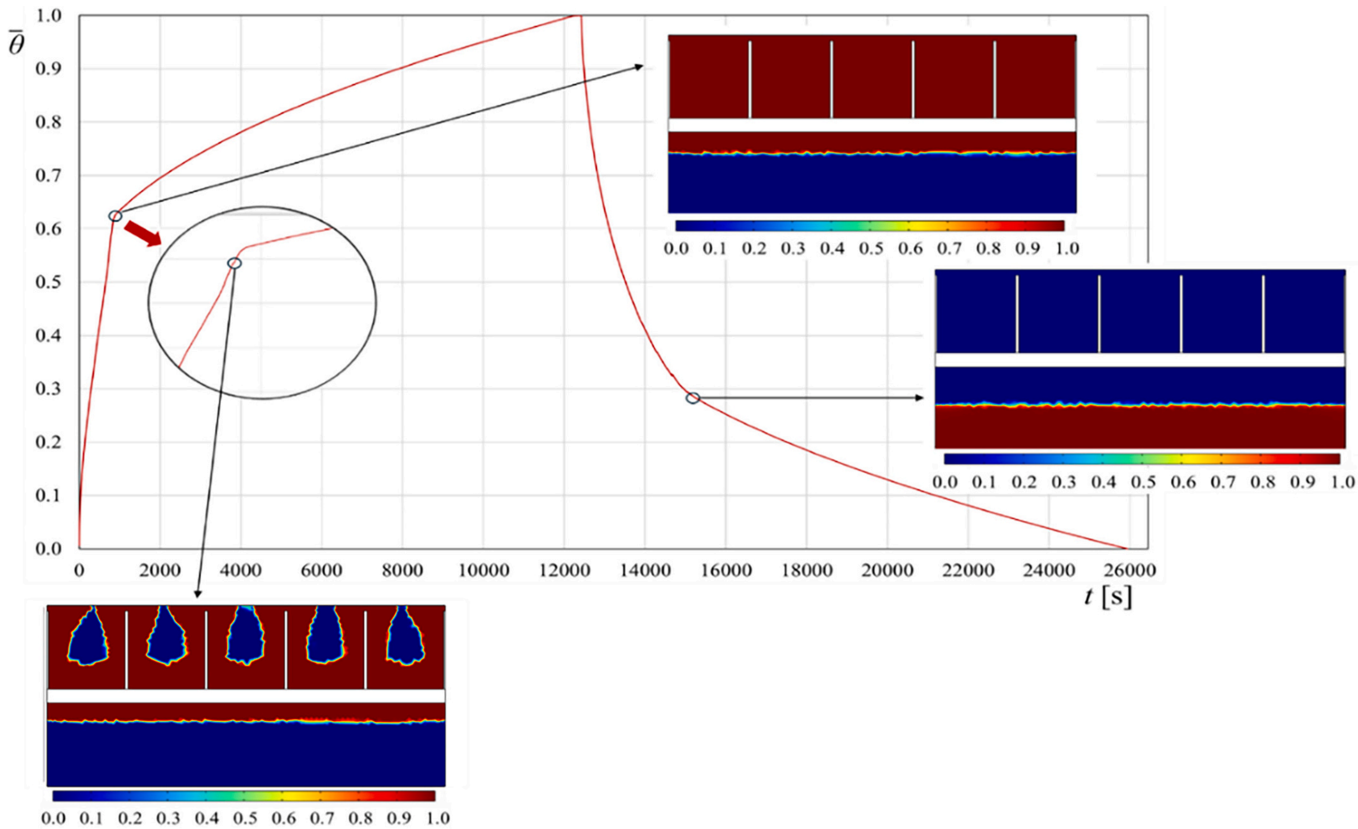

Fig. 7. Fins in the upper cavity configuration; average melting fraction as a function of time and melting fraction distribution at significant instants.

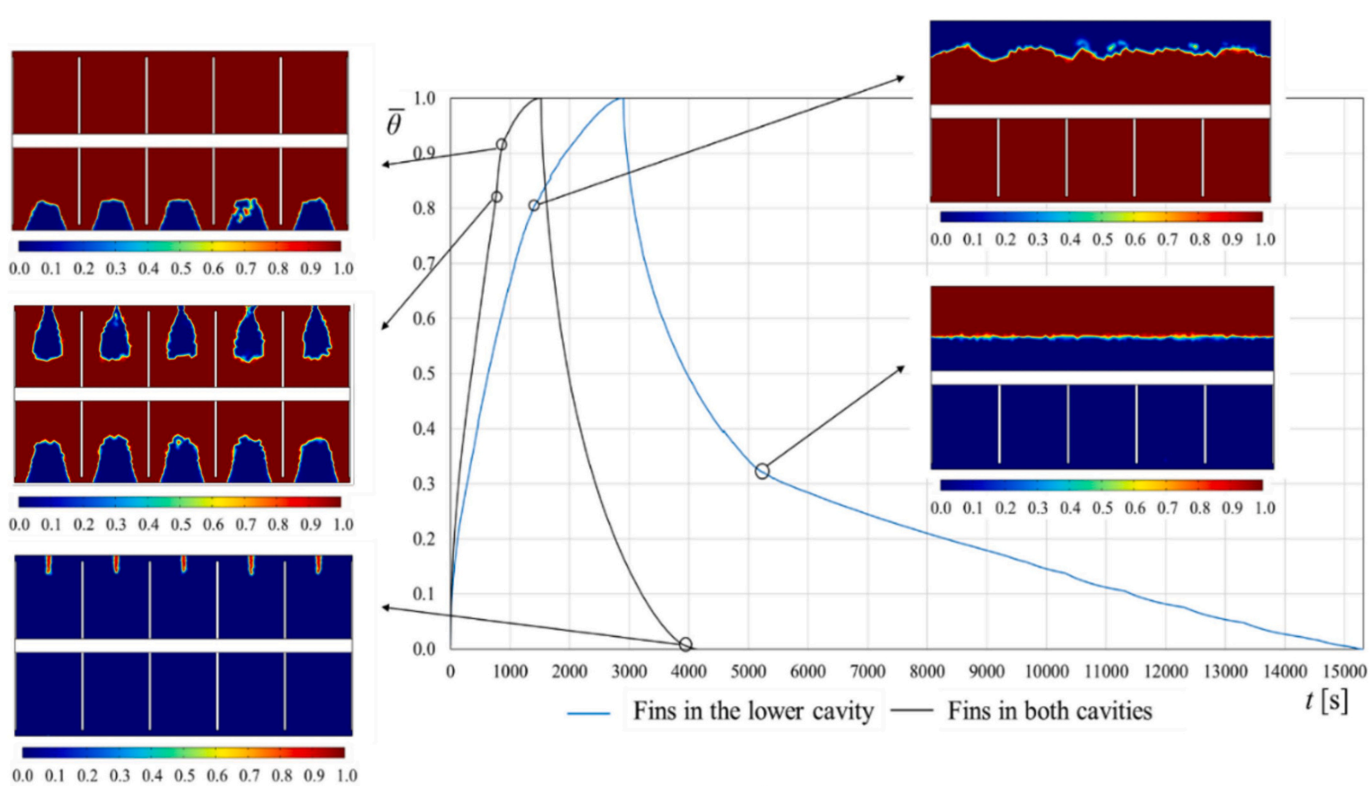

Fig. 8. Fins in the lower cavity and fins in both cavities configurations; average melting fraction as a function of time and melting fraction distribution at significant instants.

temperature distribution at the end of melting. Indeed, as the top cavity dictates in the case of the end of melting, the PCM temperature does not have time to warm further by sensible heat exchange. Thanks to the fins, solidification ends faster in the bottom cavity than in the upper one.

Finally, the case of fins in both cavities, also shown in Fig. 8, combines all the phenomena previously described, leading to the fastest melting-solidification processes. Again, vertical boundary layers develop along the fins, accelerating the PCM melting process.

4.2. Single cavity-melting and single cavity-solidification

We now consider a cycle of heat charging (melting) and heat discharging (solidification) when the temperature of the heat transfer fluid is switched from hot to cold as soon as any cavity is entirely filled with liquid PCM. We show in Figs. 9 and 10 the average temperature in time on the storage tank when each cavity contains six metallic fins. The results for the other configurations (no metallic fins, six metallic fins in the upper cavity, and six metallic fins in the lower cavity) are shown in Appendix B.

The cavity that becomes filled with fully liquid PCM is, as expected, the top one as natural convection in this bottom-heated case enhances and favors melting. This allows to switch the Heat Transfer Fluid (HTF) temperature to cold at 60% of the time that was needed when waiting to melt the entire PCM volume of the storage tank.

Note the change in shape of the average PCM temperature in the top cavity towards the end of melting. This change corresponds to the appearance of the solid drops [27] which will quickly melt once dragged to the bottom of the cavity in contact with the HTF plenum (see top right of Fig. 9).

Solidification, on the contrary to melting, takes nearly as long as in the previous case. During a quick initial phase, the now cold metallic fins help solidification in the top cavity. The behavior is similar to what was observed previously and described in the previous section. The slope of the average temperature curve changes in the vicinity of the PCM phase change temperature range, indicated by the horizontal dashed lines in Fig. 9.

In the bottom cavity melting stops at about 80%, leaving pockets of solid PCM at the very bottom of the cavity, thus opposite to the HTF location (see top right of Fig. 10). Hence, solidification starts when the liquid PCM is at a temperature still very close to the melting temperature range, facilitating the solidification process as shown by the strong initial slope in the PCM average temperature change. Because solidification is mainly a conduction process in this case, the central zone delineated by the HTF location and two metallic fins is the last to solidify.

Fig. 11 shows the liquid fraction at the end of melting (top) and at the end of solidification (bottom) when the storage tank is without fins (left) or with twelve fins (right). Note the effect of buoyancy preventing a symmetry in melting and therefore easing melting in the top cavity while preventing it in the bottom one. The reverse is true during solidification. The addition of metallic fins smoothens this lack of symmetry both in melting and in solidification phases.

4.3. Heat exchanged in melting-solidification cycles

The latent heat Q_L stored (released) during the PCM melting (solidification) is evaluated as

$$Q_L = \rho V_L L_f \tag{18}$$

where V_L is the PCM volume that is subjected to phase change, obtained as

$$\begin{aligned} V_L &= \int_V \theta dV \quad \text{melting process} \\ V_L &= \int_V (1-\theta) dV \quad \text{solidification process} \end{aligned} \tag{19}$$

where V is the volume of the cavity without that of the fins, where present, and the distribution of the liquid fraction θ is evaluated at the end of the melting (solidification) process. As a consequence, V_L coincides with the volume V occupied by the PCM in the total melting and total solidification cycle, where θ is equal to 1 (0) on the entire volume at the end of the melting (solidification) process. On the other hand, $V_L < V$ in the single cavity-melting and single cavity-solidification cycle, due to the presence of PCM that is still in the mushy region in one of the two cavities at the end of the process.

The sensible heat Q_S exchanged during the process is evaluated as

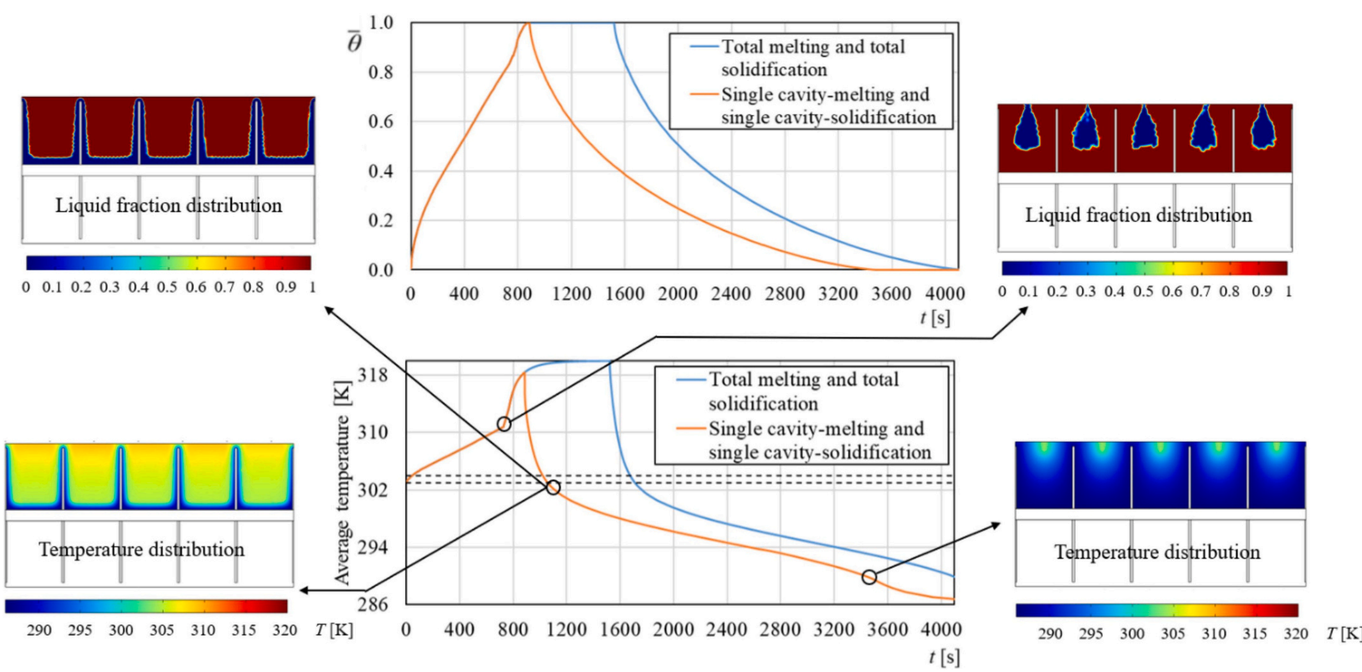

Fig. 9. Top cavity. Average liquid fraction and average temperature as a function of time, with liquid fraction and temperature distributions at significant instants. The storage unit has twelve metallic fins. The two different melting-solidification strategies are considered.

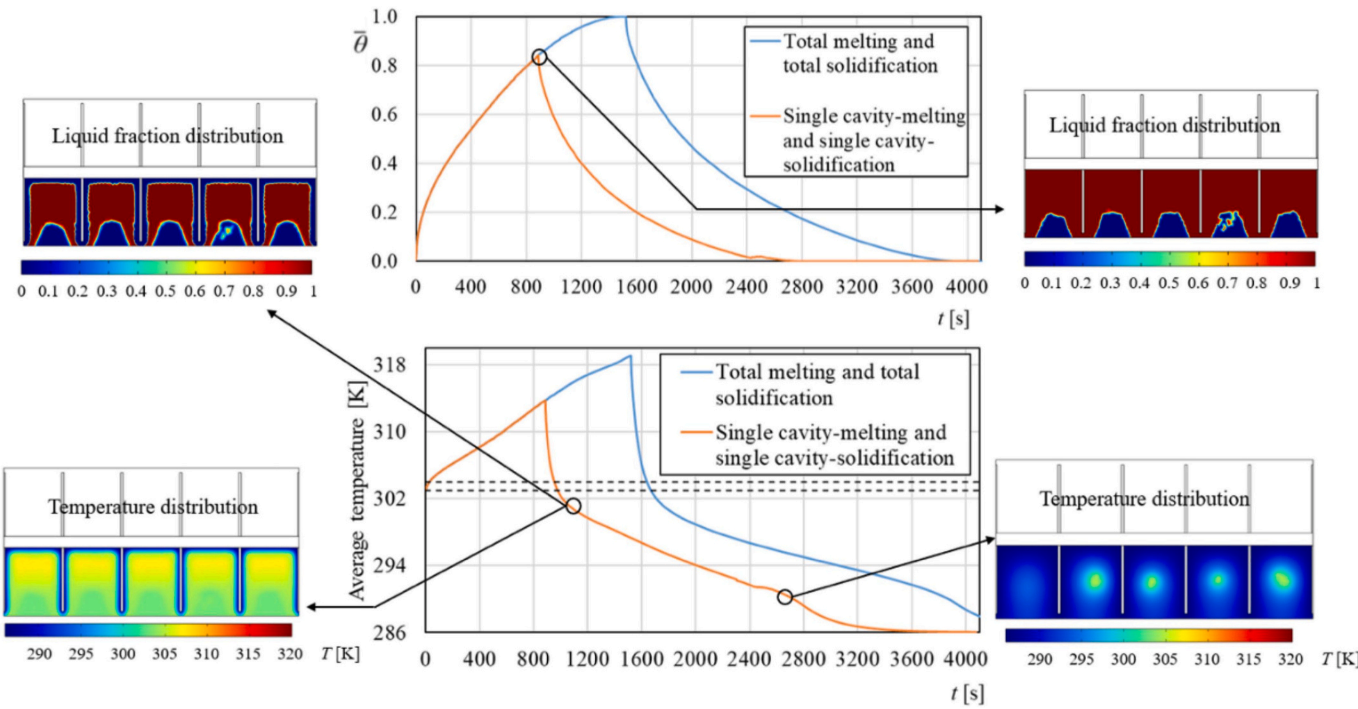

Fig. 10. Bottom cavity. Average liquid fraction and average temperature as a function of time, with liquid fraction and temperature distributions at significant instants. The storage unit has twelve metallic fins. The two different melting-solidification strategies are considered.

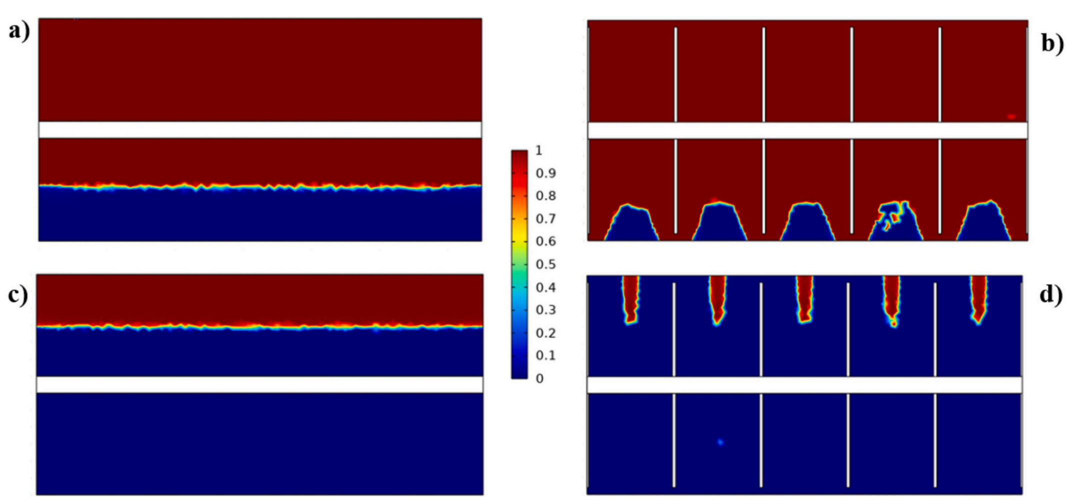

Fig. 11. Single cavity-melting and single cavity-solidification; liquid fraction distribution at the end of melting: (a) with no fins, and (b) with twelve fins; liquid fraction distribution at the end of solidification: (c) with no fins, and (d) with twelve fins.

$$Q_S = \rho V_S c_p \left(T - T_{pc,h}\right) \tag{20}$$

where V_S is the volume of the PCM that completed the phase change and is subjected to sensible heating (cooling), namely, only the zones where θ equals 1 (0) at the end of the melting (solidification) process are computed. Consequently, $V_S \leq V_L$.

The total heat Q_{TOT} stored (released) during melting (solidification) is

$$Q_{TOT} = Q_L + Q_S \tag{21}$$

Finally, the total heat exchanged during a melting-solidification cycle, $Q_{TOT,ex}$, is obtained by summing the values of Q_{TOT} of the melting and solidification processes.

The heat density is defined as the ratio of the total heat exchanged during a melting-solidification cycle ($Q_{TOT,ex}$), divided by the total PCM volume contained in the two compartments (V). To compare the results in a more general way, each heat density is expressed relatively to the no-fins total melting-total solidification base case $\left(Q_{TOT,ex}/V\right)^*$. By the same token the non-dimensional time Δt^* is calculated as the ratio of the total time of a cycle and the total time of the no-fins total melting-total solidification base case. Results are plotted in Fig. 12. All cases relative to the total melting-total solidification case align on the quasi same horizontal, as the additions of fins, wherever they are, are meant to shorten the total duration of heat absorption (PCM melting) and heat release (PCM solidification).

Conclusions are significantly different when the Heat Transfer Fluid temperature is decreased immediately after one compartment is entirely filled with liquid PCM, allowing solidification to start. First, all cases complete their melting-solidifying cycle with ~20% of the time for the

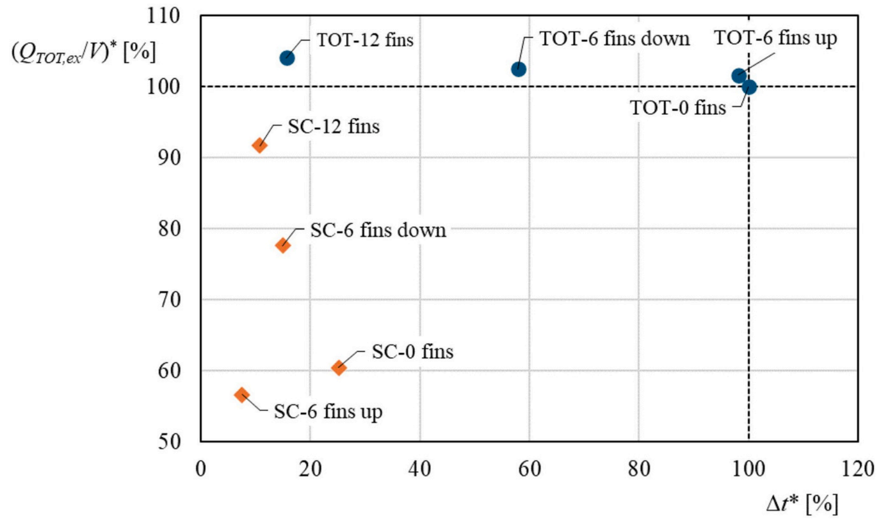

Fig. 12. Non-dimensional heat density as a function of the non-dimensional time for the various configurations; total melting and total solidification cycle (TOT), single cavity-melting and single cavity-solidification cycle (SC).

base case, even for the no-fins configuration. Because of this, the heat exchange for the latter is 60% of the base case. The configuration with 6 fins in the upper compartment generates less heat exchanges than the no-fins equivalent case. The reason comes from the fast melting in the upper compartment favored, as already mentioned, by natural convection and the metallic fins heat transfer enhancement. As the solidification phase starts right after, the PCM in the bottom compartment has very little time to contribute to the heat exchange, leading to the poorest performance in terms of total heat density exchange. Results are better when the fins are located in the bottom compartment with almost 80% of total heat density exchanged during the cycle. Finally, Fig. 12 shows a difference of only 12% in total heat density between the two 12 fins configurations highlighting the strong impact brought by the metallic fins.

5. Conclusions

This work presents a comprehensive numerical analysis of a fin-enhanced horizontal Latent Thermal Energy Storage (LTES) system highlighting the impact of metallic fins location and natural convection on the phase change dynamics during melting–solidification cycles.

The results indicate that natural convection dominates melting in the upper cavity, while the lower cavity heat exchanges remain controlled by conduction. These strongly cavity-dependent heat transfer mechanisms dictate therefore the overall cycle duration. Indeed, the addition of fins only in the upper cavity improves local thermal response but does not reduce the total melting–solidification time. When fins are located in the lower cavity, the conduction-driven process becomes less limiting and the system performance improves. The best performance is achieved when fins are installed in both cavities, resulting in the shortest cycle time.

The study also shows how to mitigate the asymmetry between melting and solidification due to buoyancy effects by means of metallic fins favoring a more uniform heat transfer. In partial-cycle operation, switching the HTF temperature when a single cavity completes melting allows to reduce the total cycle time. However, competing trends between speed and stored/released energy, require an optimal position of fins, particularly in the lower cavity. The optimal fin location is not uniform in the storage tank but must target the thermally limiting region of the system. These results contribute to the design of advanced LTES systems with improved efficiency, reduced operating times, and improved thermal performance for energy storage applications.

CRediT authorship contribution statement

Claudia Naldi: Writing – original draft, Software, Methodology, Investigation, Funding acquisition, Formal analysis, Data curation, Conceptualization. **Giulia Martino:** Visualization, Validation, Software, Data curation. **Cesare Biserni:** Writing – review & editing, Resources, Funding acquisition, Formal analysis. **Sylvie Lorente:** Writing – original draft, Supervision, Project administration, Methodology, Investigation, Formal analysis, Conceptualization.

Declaration of competing interest

The authors declare the following financial interests/personal relationships which may be considered as potential competing interests:

Given their role as members of the Editorial Board, S. Lorente and C. Biserni had no involvement in the peer review of this article and had no access to information regarding its peer review. Full responsibility for the editorial process for this article was delegated to another journal editor. If there are other authors, they declare that they have no known competing financial interests or personal relationships that could have appeared to influence the work reported in this paper.

Acknowledgements

This paper was supported by the Emilia-Romagna Regional Development Fund PR-FESR 2021-2027 Program under the project SACER, CUP J47G22000760003, and by the Piano Triennale della Ricerca di Sistema Elettrico PTR 2025-2027, Project 1.5, LA2.12, CUP I53C24003330001. Sylvie Lorente wants to thank the Institute of Advanced Studies of the University of Bologna for hosting her as Visiting Fellow. This work is one of the outcomes of the resulting collaboration.

Appendix A

The assumption of uniform temperature for the heat transfer fluid considered in this work was validated by performing several simulations of the heat transfer fluid laminar flow along the mid-height channel, with a given inlet temperature and different mass flow rates. The obtained values of temperature decrease of the heat transfer fluid between inlet and outlet at 1500 s, shown in Fig. A.1 as a function of the Reynolds number, become negligible at medium-high *Re*, confirming the validity of the assumption.

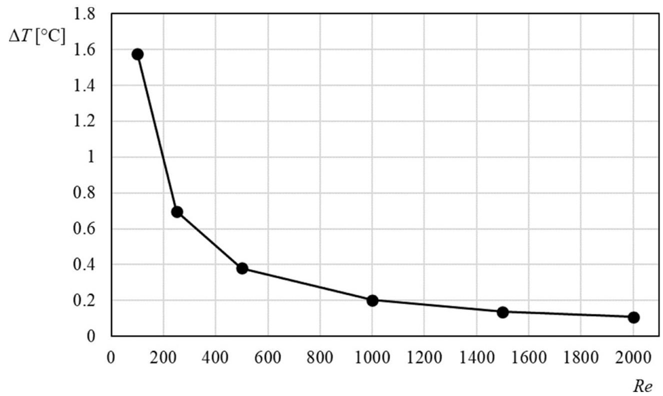

Fig. A.1. Temperature decrease of the heat transfer fluid between the inlet and outlet of the mid-height channel at 1500 s as a function of the Reynolds number.

Appendix B

This section includes the time evolution of the average liquid fraction and of the average temperature, for the cases with: no fins, fins in the top cavity only, fins in the bottom cavity only. The PCM phase change temperature range is highlighted by the horizontal dashed lines.

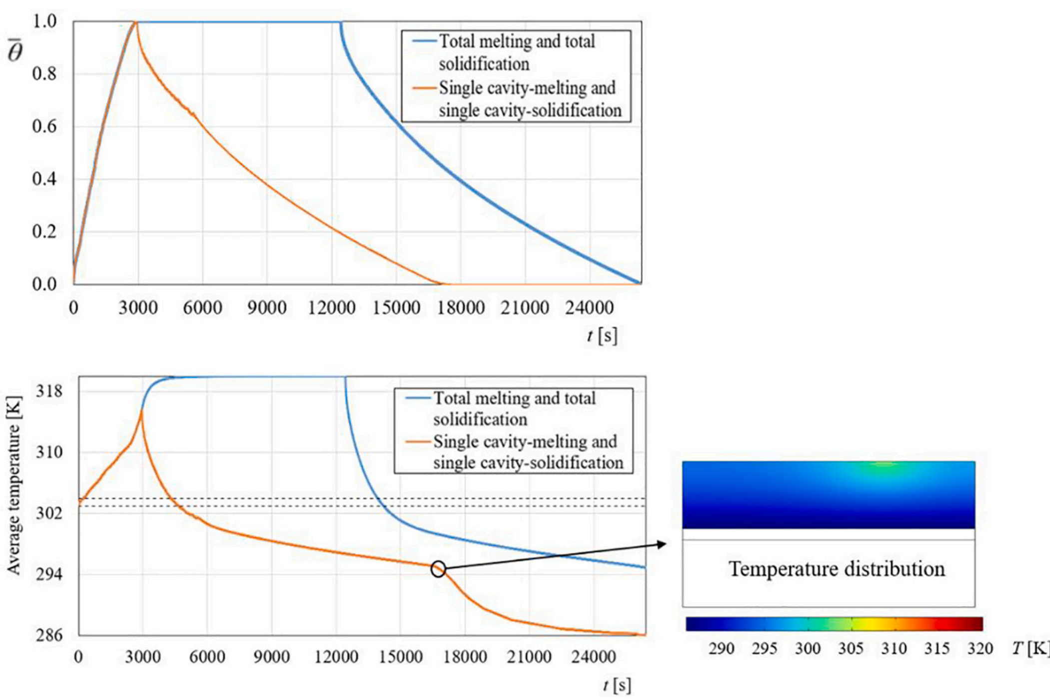

Fig. B.1. Top cavity. Average liquid fraction and average temperature as a function of time, with temperature distribution at significant instant. The storage unit has no metallic fins. The two different melting-solidification strategies are considered.

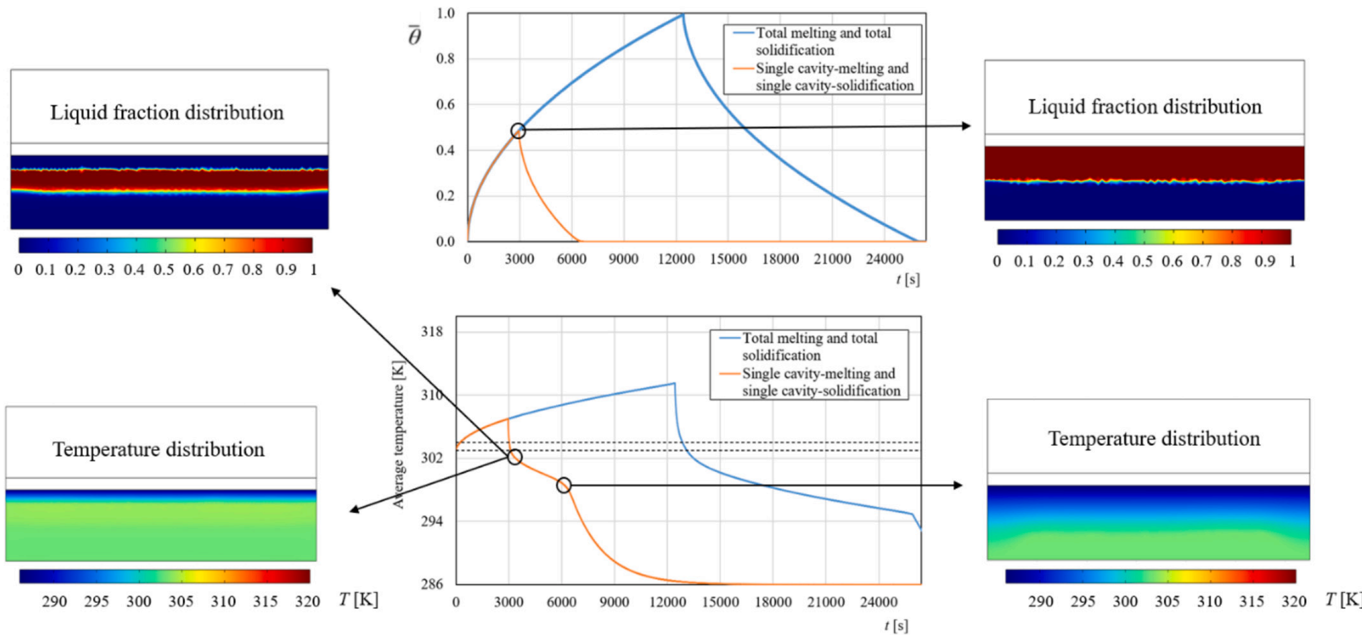

Fig. B.2. Bottom cavity. Average liquid fraction and average temperature as a function of time, with liquid fraction and temperature distributions at significant instants. The storage unit has no metallic fins. The two different melting-solidification strategies are considered.

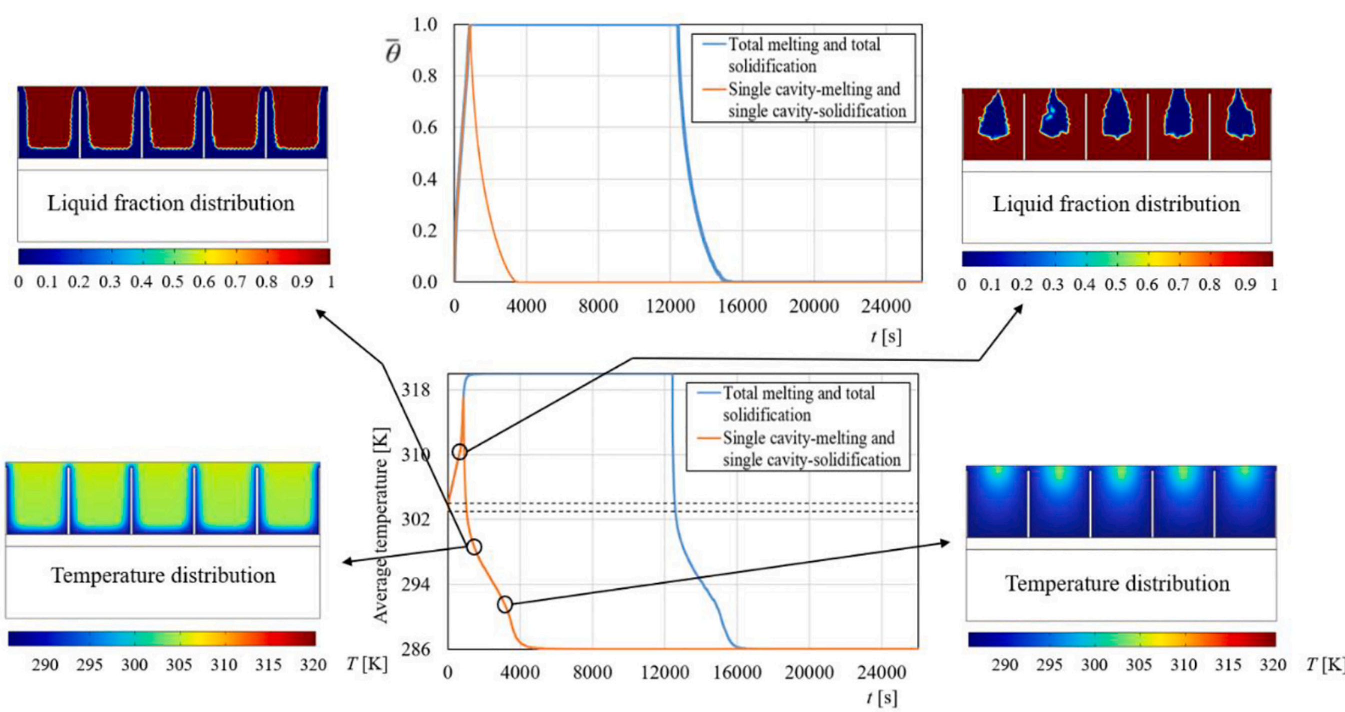

Fig. B.3. Top cavity. Average liquid fraction and average temperature as a function of time, with liquid fraction and temperature distributions at significant instants. The storage unit has six metallic fins in the upper cavity. The two different melting-solidification strategies are considered.

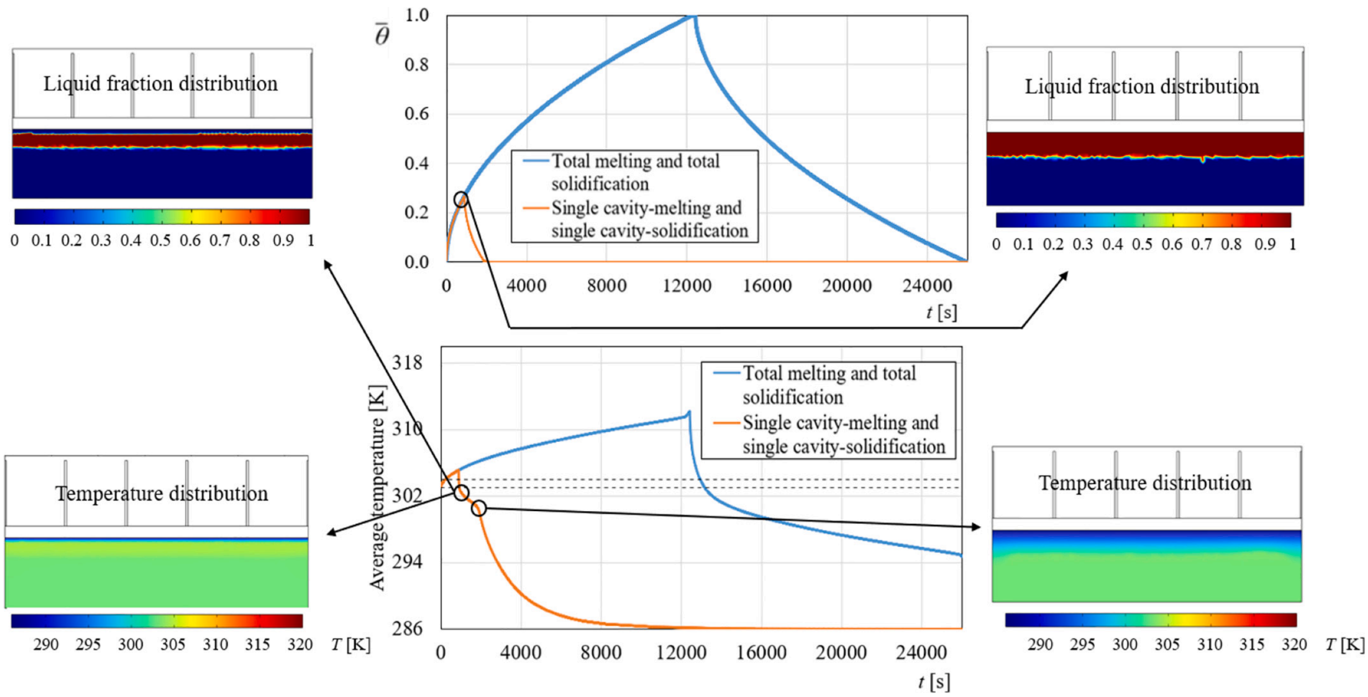

Fig. B.4. Bottom cavity. Average liquid fraction and average temperature as a function of time, with liquid fraction and temperature distributions at significant instants. The storage unit has six metallic fins in the upper cavity. The two different melting-solidification strategies are considered.

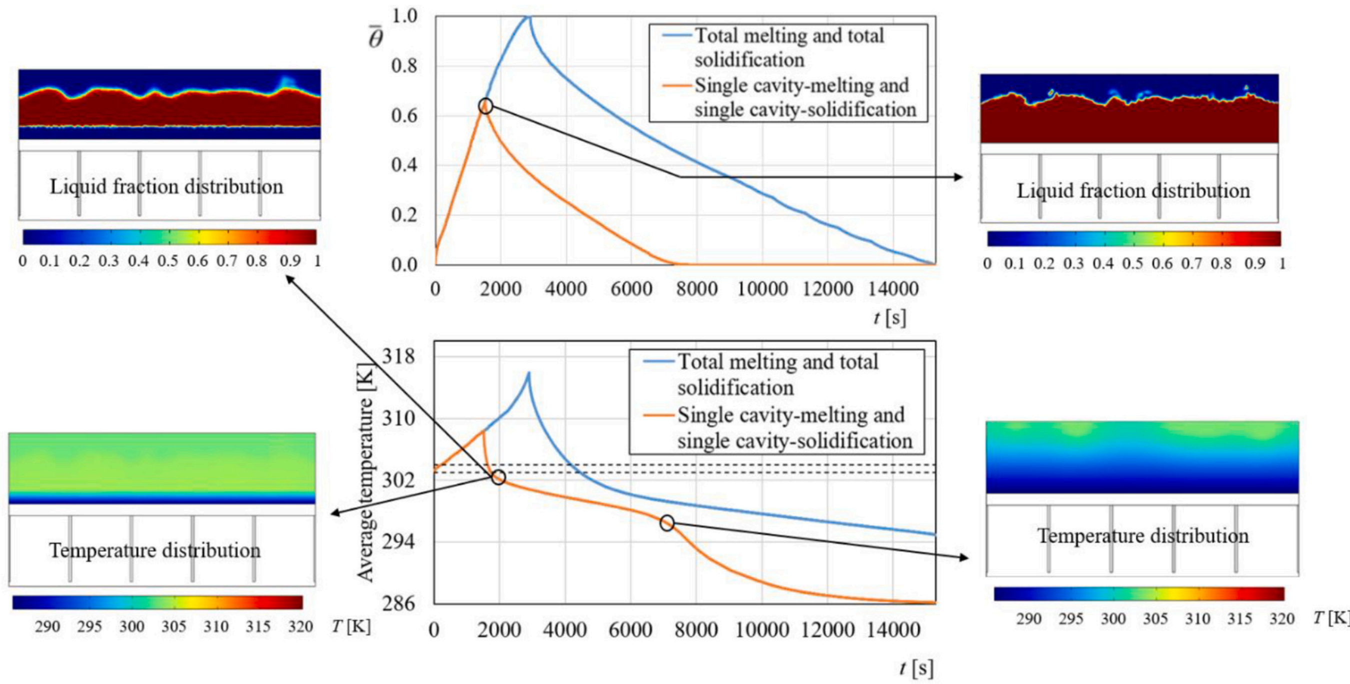

Fig. B.5. Top cavity. Average liquid fraction and average temperature as a function of time, with liquid fraction and temperature distributions at significant instants. The storage unit has six metallic fins in the lower cavity. The two different melting-solidification strategies are considered.

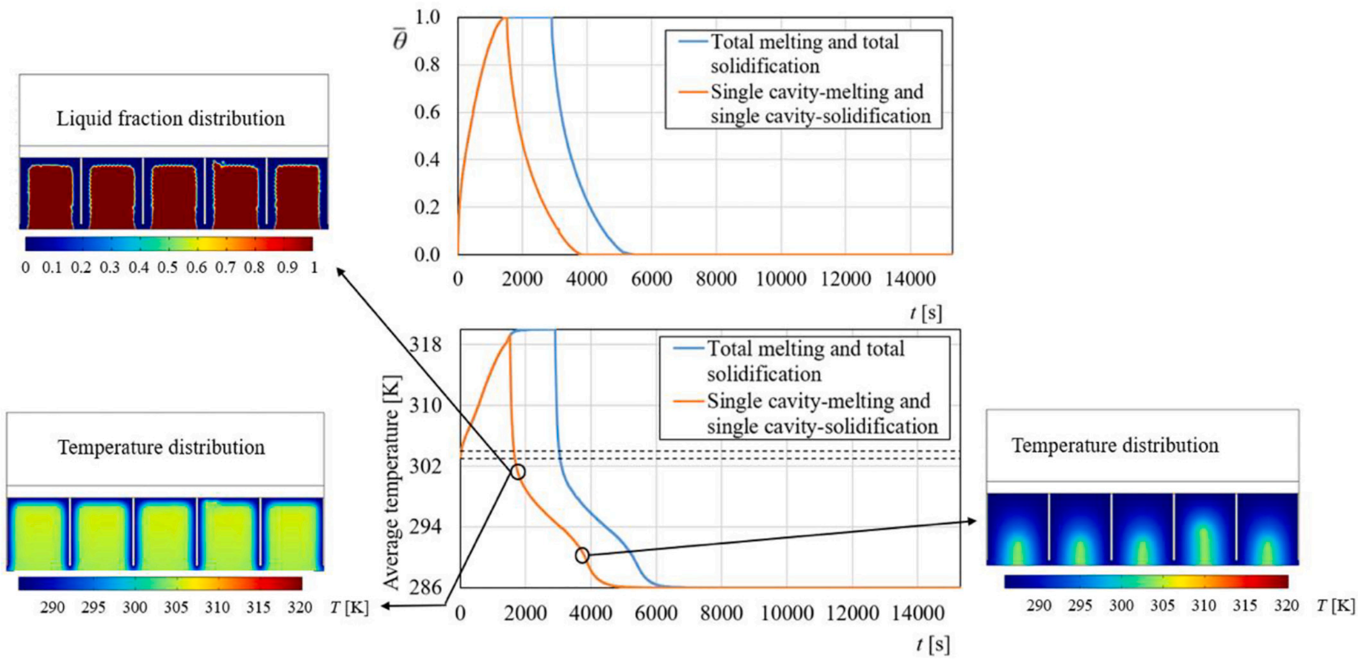

Fig. B.6. Bottom cavity. Average liquid fraction and average temperature as a function of time, with liquid fraction and temperature distributions at significant instants. The storage unit has six metallic fins in the lower cavity. The two different melting-solidification strategies are considered.

Data availability

Data will be made available on request.

References

[1] F.L. Rashid, M.A. Al-Obaidi, A. Dulaimi, H.Y. Bahlol, A. Hasan, Recent advances, development, and impact of using phase change materials as thermal energy storage in different solar energy systems: a review, Designs 7 (2023) 66.

[2] J. Wu, N. Li, Z. Wu, Experimental investigation of latent energy storage systems with the tree-pin-shaped fin, Appl. Therm. Eng. 227 (2023) 120370.

[3] R.D.C. Oliveski, F. Becker, L.A.O. Rocha, C. Biserni, G.E.S. Eberhardt, Design of fin structures for phase change material (PCM) melting process in rectangular cavities, J. Energy Storage 35 (2021) 102337.

[4] G. Righetti, C. Zilio, G.A. Longo, K. Hooman, S. Mancin, Experimental study on the effect of metal foams pore size in a phase change material based thermal energy storage tube, Appl. Therm. Eng. 217 (2022) 119163.

[5] X. Wei, N. Zhang, Z. Zhang, X. Cao, Y. Yuan, Melting evaluation of phase change materials impregnated into cascaded metal foams with regionalized enhancement, J. Therm. Sci. 34 (2025) 223–241.

[6] C. Yadav, R.R. Sahoo, Thermal analysis comparison of nano additive PCM based engine waste heat recovery thermal storage systems: an experimental study, J. Therm. Anal. Calorim. 147 (2022) 2785–2802.

[7] A.H. Eisapour, M. Eisapour, H.I. Mohammed, A.H. Shafaghat, M. Ghalambaz, P. Talebizadehsardari, Optimum design of a double elliptical latent heat energy storage system during the melting process, J. Energy Storage 44 (2021) 103384.

[8] M.A. Khuda, N. Sarunac, A comparative study of latent heat thermal energy storage (LTES) system using cylindrical and elliptical tubes in a staggered tube arrangement, J. Energy Storage 87 (2024) 111333.

[9] S. Ziaei, S. Lorente, A. Bejan, Constructal design for convection melting of a phase change body, Int. J. Heat Mass Transf. 99 (2016) 762–769.

[10] A.J. Khosroshahi, S. Hossainpour, Investigation of storage rotation effect on phase change material charging process in latent heat thermal energy storage system, J. Energy Storage 36 (2021) 102442.

[11] Z. Shen, S. Chen, B. Chen, Heat transfer performance of a finned shell-and-tube latent heat thermal energy storage unit in the presence of thermal radiation, J. Energy Storage 45 (2022) 103724.

[12] H. Kim, J. Hong, H. Choi, J. Oh, H. Lee, Development of PCM-based shell-and-tube thermal energy storages for efficient EV thermal management, Int. Commun. Heat Mass Transfer 154 (2024) 107401.

[13] U. Srivastava, R.R. Sahoo, Rayleigh-Bénard and melting effects on hybrid phase change materials for fin orientation-based triple tube thermal energy storage system, Int. Commun. Heat Mass Transfer 176 (2026) 111392.

[14] F. Ren, J. Du, X. Yang, X. Huang, Optimization on a novel irregular snowflake fin for thermal energy storage using response surface method, Int. J. Heat Mass Transf. 200 (2023) 123521.

[15] A. Arshad, A phase change material-based constructal design finned heat sink: an evolutionary design for thermal management, Int. Commun. Heat Mass Transfer 161 (2025) 108379.

[16] A.E. Amer, A. Ahmed, T. Nabil, A.A. Ezat, A. Refaat, A.E. Khalifa, M. Elgamal, M. Elsakka, Performance evaluation of latent heat storage unit using novel hook-shaped fins: experimental investigation, J. Energy Storage 97 (2024) 112747.

[17] C. Xiao, T. Xie, X. Huang, Y. Wang, Y. Hong, J. Du, Energy storage and thermodynamic characteristics in a finned rectangular latent thermal storage unit with multiple enclosures, Int. Commun. Heat Mass Transfer 176 (2026) 111294.

[18] X. Jia, X. Zhai, X. Cheng, Thermal performance analysis and optimization of a spherical PCM capsule with pin-fins for cold storage, Appl. Therm. Eng. 148 (2019) 929–938.

[19] X. Zhang, S. Lorente, A.P. Wemhoff, Modeling the thermal energy storage capability of a phase change material confined in a rectangular cavity, Int. Commun. Heat Mass Transfer 126 (2021) 105367.

[20] W. Ge, J. Zou, X. Meng, Thermal performance improvement of spherical encapsulated phase-change material by the metal fins, Energy Rep. 13 (2025) 2384–2392.

[21] H. Liu, Y. Hu, G. Yang, C. Wu, Y. Li, PCM melting characteristics in a sidewall-heated rectangular cavity with non-uniform longitudinal fins near the bottom, Renew. Energy 242 (2025) 122451.

[22] B. Lu, Y. Zhang, Z. Wang, J. Zhu, J.Z.D. Sun, Effect of shell shape on the charging and discharging performance of a vertical latent heat thermal energy storage unit: an experimental study, J. Energy Storage 56 (2022) 105996.

[23] B. Medjahed, M. Arıcı, S. Dardouri, S. Chaib, O.E. Goual, A. Yüksel, Experimental analysis of the thermal performance of beeswax-heat exchanger as latent heat thermal energy storage system, J. Energy Storage 101 (2024) 113898.

[24] D.S. Mehta, K. Solanki, M.K. Rathod, J. Banerjee, Thermal performance of shell and tube latent heat storage unit: comparative assessment of horizontal and vertical orientation, J. Energy Storage 23 (2019) 344–362.

[25] W.A. Dukhan, N.S. Dhaidan, T.A. Al-Hattab, Experimental investigation of the horizontal double pipe heat exchanger utilized phase change material, Mater. Sci. Eng. 671 (2020) 012148.

[26] G.S. Sodhi, V. Kumar, P. Muthukumar, Design assessment of a horizontal shell and tube latent heat storage system: alternative to fin designs, J. Energy Storage 44 (2021) 103282.

[27] C. Naldi, G. Martino, M. Dongellini, S. Lorente, Rayleigh–Bénard type PCM melting and solid drops, Int. J. Heat Mass Transf. 218 (2024) 124767.

[28] S. Ziaei, S. Lorente, A. Bejan, Morphing tree structures for latent thermal energy storage, J. Appl. Phys. 117 (2015) 224901, https://doi.org/10.1063/1.4921442.

[29] O. Bertrand, B. Binet, H. Combeau, S. Couturier, Y. Delannoy, D. Gobin, M. Lacroix, P. Le Quere, M. Medale, J. Mencinger, H. Sadat, G. Vieira, Melting driven by natural convection - a comparison exercise: first results, Int. J. Therm. Sci. 38 (1999) 5–26.

[30] F.L. Tan, S.F. Hosseinizadeh, J.M. Khodadadi, L. Fan, Experimental and computational study of constrained melting of phase change materials (PCM) inside a spherical capsule, Int. J. Heat Mass Transf. 52 (2009) 3464–3472.

[31] N. Bianco, A. Fragnito, M. Iasiello, G.M. Mauro, L. Mongibello, Multi-objective optimization of a phase change material-based shell-and-tube heat exchanger for cold thermal energy storage: experiments and numerical modeling, Appl. Therm. Eng. 215 (2022) 119047.
[32] COMSOL Multiphysics. https://www.comsol.com/, 2026 (last accessed on May 21, 2026).
[33] W. Guo, R. Zhao, Y. Liu, D. Huang, Semi-theoretical correlations of melting process driven by Rayleigh–Bénard convection suitable for low melting point metal, Case Stud. Therm. Eng. 28 (2021) 101511.
[34] P.H. Biwole, D. Groulx, F. Souayfane, T. Chiu, Influence of fin size and distribution on solid-liquid phase change in a rectangular enclosure, Int. J. Therm. Sci. 124 (2018) 433–466.
[35] B. Kiyak, H.F. Oztop, N. Biswas, F. Selimefendigil, Effects of geometrical configurations on melting and solidification processes in phase change materials, Appl. Therm. Eng. 258 (2025) 124726.